PAPER

Etched and doped Co$_9$S$_8$/graphene hybrid for oxygen electrocatalysis†

Shuo Dou,[a] Li Tao,[a] Jia Huo,[a] Shuangyin Wang*[a] and Liming Dai[b]

Highly efficient electrocatalysts for the oxygen reduction reaction (ORR) and oxygen evolution reaction (OER) have been regarded as the core elements in a wide range of renewable energy technologies. Surface engineering of the electrocatalysts is one of the most popular strategies to improve their catalytic activity. Herein, we, for the first time, designed an advanced bi-functional electrocatalyst for the ORR and OER by simultaneously etching and doping a cobalt sulfides–graphene hybrid with NH$_3$-plasma. The graphene supported Co$_9$S$_8$ nanoparticles were prepared (denoted as Co$_9$S$_8$/G) first, followed by the NH$_3$-plasma treatment, which could not only lead to nitrogen doping into both Co$_9$S$_8$ and graphene, but also partially etch the surface of both Co$_9$S$_8$ and graphene. The heteroatom doping could efficiently tune the electronic properties of Co$_9$S$_8$ and graphene, and the surface etching could expose more active sites for electrocatalysis, which can contribute significantly to the enhanced electrocatalytic performance for ORR and OER. The electrochemical results revealed that the etched and N-doped Co$_9$S$_8$/G shows excellent ORR activity, which is close to that of the commercial Pt/C catalyst, and great OER activity. The strategy developed here provides a novel and efficient approach to prepare hybrid bi-functional electrocatalysts for ORR and OER.

Broader context

Oxygen reduction reaction (ORR) and oxygen evolution reaction (OER) are the most important processes in a wide range of renewable-energy technologies, such as in fuel cells, metal–air batteries, and water splitting devices. In this study, NH$_3$-plasma was employed to treat graphene supported Co$_9$S$_8$ nanoparticles as an efficient bi-functional electrocatalyst for ORR and OER. During the plasma process at high temperature, simultaneous doping and etching occurs on the surface of the Co$_9$S$_8$–graphene hybrid. NH$_3$-plasma could induce *N* atom doping into both Co$_9$S$_8$ and graphene to obtain N-doped Co$_9$S$_8$ and N-doped graphene in the hybrid, which efficiently tunes the electronic properties of Co$_9$S$_8$ and graphene. On the other hand, the plasma treatment can also realize the surface etching of the Co$_9$S$_8$ nanoparticles and graphene nanosheets, which results in the exposure of more active sites for electrocatalysis. By the advanced strategy developed here, the as-prepared etched and doped Co$_9$S$_8$/graphene hybrid exhibits excellent ORR and OER activities, which are comparable to the state-of-the-art Pt/C and RuO$_2$ catalysts. Furthermore, the novel NH$_3$-plasma process provides a novel and efficient approach to prepare hybrid bi-functional electrocatalysts for ORR and OER.

Introduction

The impending global energy crisis caused by the heavy reliance upon traditional fossil fuels encourages researchers to search for possible renewable energy strategies, including fuel cells, metal–air batteries and water splitting devices.[1–4] The electrochemical oxygen reduction reaction (ORR) and oxygen evolution reaction

(OER) have been regarded as two of the most important processes in a wide range of the above renewable-energy technologies.[5–8] However, both ORR and OER are kinetically challenging, thus demanding highly effective electrocatalysts. More critically, the development of bi-functional electrocatalysts for both ORR and OER is of critical importance for the development of electrochemical devices, especially for rechargeable metal–air batteries.[9] Platinum (Pt) and Pt-based materials are the most efficient ORR catalysts because of their low onset potential and high current density. For OER, ruthenium oxide (RuO$_2$) and iridium oxide (IrO$_2$), are usually considered as the best electrocatalysts.[10,11] But, these noble-metal materials suffer from high cost and scarcity on the earth. Additionally, the capability of Pt or RuO$_2$/ IrO$_2$ for simultaneously catalyzing ORR and OER is very poor,

[a] *State Key Laboratory of Chem/Bio-Sensing and Chemometrics, College of Chemistry and Chemical Engineering, Hunan University, Changsha, 410082, P. R. China. E-mail: shuangyinwang@hnu.edu.cn*
[b] *Department of Macromolecular Science and Engineering, Case Western Reserve University, Cleveland, OH, 41006, USA*
† Electronic supplementary information (ESI) available. See DOI: 10.1039/c6ee00054a

since Pt is only active for ORR but inactive for OER and RuO_2/IrO_2 is only active for OER but inactive for ORR.[12] Therefore, the development of non-noble metal and efficient bi-functional electrocatalysts towards both ORR and OER is of high demand.

Recently, many kinds of bi-functional electrocatalysts have been explored. For example, the alloy of Pt and Ir/Ru was shown to exhibit high catalytic activity towards ORR and OER.[13–15] But the use of noble metals still limits its large-scale application in electrochemical energy devices. Since we reported the nitrogen-doped carbon nanotube as a highly efficient metal-free ORR electrocatalyst in 2009, heteroatom-doped carbon nanomaterials have been confirmed to be an efficient ORR electrocatalyst.[16] Recently, we successfully developed B- and N-doped carbon and sulfur-doped graphene through various strategies, showing good electrocatalytic performance for ORR.[17–19] On the other hand, while active for ORR, the heteroatom-doped carbon materials also show possible OER activity as discovered recently.[20–22] The earth abundant carbon materials can lower the cost compared to the noble metal alloys for practical application. However, the OER activity on the heteroatom-doped carbon materials is still sluggish even though the ORR activity could catch up with the commercial Pt/C catalyst. In order to address this question, the composite of cobalt (Co)-based compound (such as cobalt oxide, cobalt sulfide) and carbon materials has been proposed to actively catalyze OER with low overpotential and high durability.[23,24] It has been reported that the synergetic chemical coupling between Co_3O_4 and graphene could effectively enhance the electrocatalytic performance for ORR and OER.[25] Meanwhile, Co_9S_8 on graphene has also been proved to be efficient electrocatalysts for ORR and OER.[26–28] Metal doping in Co-based compounds (*e.g.* $NiCo_2O_4$, $NiCo_2S_4$) on carbon materials is another approach to further enhance the catalytic activity.[29,30] However, there are rarely studies about non-metal atoms (anion)-doped Co-based compounds on carbon to be used as bi-functional electrocatalysts. Previously, we successfully prepared oxygen doped MoS_2 as highly efficient electrocatalysts for hydrogen evolution, indicating that the anion doping may be a possible approach to tune the electronic properties and thus the electrocatalytic properties of transition metal sulfides.[31] Besides, as we previously demonstrated in a self-designed micro-droplet electrochemistry system, the edge of graphite is more active than the basal plane for ORR.[32] Therefore, the surface engineering (such as etching and edging) of electrocatalysts could also efficiently tune their activity.

In this study, we, for the first time, realized the simultaneous etching and N-doping of the hybrid Co_9S_8/graphene electrocatalysts by NH_3-plasma treatment (the product was denoted as N-Co_9S_8/G). On one hand, the NH_3-plasma could induce the N doping into both Co_9S_8 and graphene to obtain N-doped Co_9S_8 and N-doped graphene in the hybrid. The N doping in carbon is an effect way to change the charge density and spin density of carbon atoms in carbon nanomaterials to enhance the electrocatalytic activity.[33,34] The N doping could also improve the electrical conductivity of metal compounds to enhance the electrocatalytic performance.[35,36] On the other hand, the NH_3-plasma treatment can also realize the surface etching on the Co_9S_8 nanoparticles and graphene nanosheets, exposing more active sites for ORR and OER.

The synergistic effect of nitrogen doping and surface etching brings us a highly efficient bi-functional electrocatalyst for ORR and OER. The as-prepared N-Co_9S_8/G reveals robust ORR performance, which has a similar onset potential and current density to the commercial Pt/C. Meanwhile, the OER activity of N-Co_9S_8/G is also impressive as the overpotential is only 0.409 V at the current density of 10 mA cm^{-2}. Overall, the strategy developed here provides a novel and efficient approach to design hybrid bi-functional electrocatalysts for ORR and OER.

Experimental

Preparation of N-Co_9S_8/G

Graphene oxide (GO) was synthesized according to a modified Hummers method which was described in our previous study.[37] 200 mg of GO was dispersed in 50 mL of water by ultrasonication for 1 h to form a homogeneous GO suspension. 10 mL of 0.28 mol L^{-1} sodium sulphide (Na_2S) solution was added to the above graphene dispersion followed by ultrasonication for 10 min. Then, the mixture was transferred to a 50 mL Teflon-sealed autoclave and 10 mL of 0.31 mol L^{-1} cobalt nitrate (Co(NO$_3$)$_2$) solution was poured in with gentle stirring and a black gel was formed. The hydrothermal reaction was carried out at 120 °C for 3 h to obtain graphene supported Co_9S_8 (Co_9S_8/G). The precipitate was washed with water and ethanol three times. The resulting Co_9S_8/G was collected after lyophilisation. The nitrogen doping and etching process was conducted in a plasma enhanced tube furnace. In brief, the as-prepared Co_9S_8/G was placed at the centre of the tube furnace and heated to 700 °C at a heating rate of 10 °C min^{-1} under NH_3 flow. For the plasma treatment, the RF power was 200 W, the pressure was 90 Pa, and the treatment time was 1 h. Similarly, N-doped graphene as well as unsupported N-doped Co_9S_8 were prepared by the same method in the absence of Co(NO$_3$)$_2$ and GO, respectively. To analyze the effect of NH_3-plasma, the non-modified Co_9S_8/G and unsupported Co_9S_8 samples were also annealed at 700 °C under an Ar atmosphere. The Co_9S_8/G was also annealed under NH_3 and was treated by 50% NH_3-plasma to investigate the effect of plasma and the influence of N doping, respectively.

Physical characterization

The morphology of the as-prepared N-Co_9S_8/graphene was observed by a scanning electron microscope (SEM, Hitachi, S-4800) and a transmission electron microscope (TEM, FEI, F20 S-TWIX). X-ray photoelectron spectroscopic (XPS) measurements were carried out with an ESCALAB 250Xi using a monochromic Al X-ray source (200 W, 20 eV). The X-ray diffraction (XRD) measurements used a Rigaku D/MAX 2500 diffractometer with Cu Kα radiation. The Raman spectra were collected on a Raman spectrometer (Labram-010) using 532 and 632 nm laser. The thermogravimetric analysis (TGA) was carried out by a STA449C instrument with a heating rate of 10 °C min^{-1} from the room temperature to 800 °C in air.

Electrochemical measurements

The ORR and OER performance of N-Co_9S_8/G was measured on an electrochemical workstation (CHI 760E, CH Instrument) and

This journal is © The Royal Society of Chemistry 2016

Energy Environ. Sci., 2016, **9**, 1320–1326 | **1321**

a rotating ring disk electrode apparatus (RRDE-3A, ALS) in a three-electrode cell by using a platinum wire as counter electrode and saturated calomel electrode (SCE) as reference electrode. The working electrode was a rotating ring/disk electrode with glass carbon disk (4 mm in diameter). To prepare the catalyst slurry, 4.0 mg of electrocatalyst was dispersed in 2 mL ethanol and 0.1 mL Nafion solution (5 wt%, Sigma Aldrich) and ultrasonicated for 60 min. 13 µL of the ink was dropped onto the glassy carbon electrode to give a catalyst loading of 0.2 mg cm^{-2} and dried in air.

The RHE calibration was conducted according to the previous work.[25] The result was illustrated in Fig. S1 (ESI†). In brief, 0.1 M KOH electrolyte was saturated with high purity hydrogen and Pt wire was used as the working electrode. CVs were performed with a scan rate of 1 mV s^{-1} from −1.0 to −0.9 V. When the current was 0 mA, two potentials would be obtained and the average value (0.99 V) of the potentials was the thermodynamic potential for the hydrogen electrode reactions. So, it could be deduced with the equation: $E(\text{RHE}) = E(\text{SCE}) + 0.99$ V.

Results and discussion

The preparation process of N-Co$_9$S$_8$/G is illustrated in Scheme 1 and the detailed method can be found in the Experimental section. Briefly, Na$_2$S and Co(NO$_3$)$_2$ were used as the S and Co sources, respectively. The Co$_9$S$_8$/G hybrid was obtained by hydrothermal synthesis. Subsequently, the Co$_9$S$_8$/G hybrid was subjected to NH$_3$-plasma treatment to realize the simultaneous etching and N doping to obtain N-doped Co$_9$S$_8$ on N doped graphene (N-Co$_9$S$_8$/G). The morphology change of the Co$_9$S$_8$/G before and after NH$_3$-plasma treatment was observed with TEM and SEM. Fig. 1a and b show the TEM images of Co$_9$S$_8$/G and N-Co$_9$S$_8$/G. It can be observed that, after the NH$_3$-plasma treatment, the distribution density of the Co$_9$S$_8$ nanoparticles on graphene obviously decreases due to the etching effect by plasma, indicating that the Co$_9$S$_8$ nanoparticles were partially etched. For the graphene substrate, it can be seen that some nanosized holes on the graphene surface (partially highlighted with red open circles) are generated in N-Co$_9$S$_8$/G, also resulting from the NH$_3$-plasma etching effect. The etching could increase the number of active sites on the graphene, which could provide low-resistant diffusion
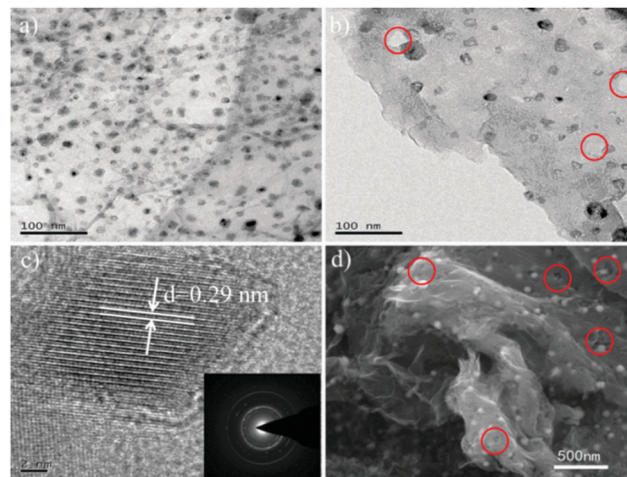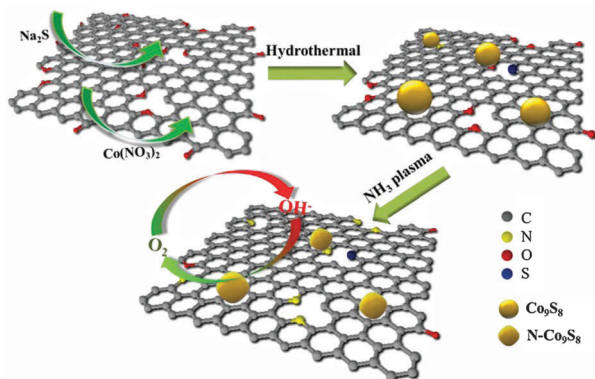

Fig. 1 TEM images of Co$_9$S$_8$/G (a) and N-Co$_9$S$_8$/G (b); (c) the HRTEM image and SAED pattern (inset) of N-Co$_9$S$_8$/G; and (d) the SEM image of N-Co$_9$S$_8$/G.

channels for O$_2$ and electrolyte, thereby improving the electrochemical performance.[38] Furthermore, the TEM image of NG was also obtained and is shown in Fig. S2 (ESI†). The nanosized hole could be seen on the surface of the graphene sheet, which further indicates the etching effect of the plasma process.

In addition, the high-resolution transmission electron microscopy (HRTEM) image is shown in Fig. 1c, where lattice fringes with a d-spacing of 0.29 nm are observed, corresponding to the (311) plane of Co$_9$S$_8$. It is also interesting to observe that, after the plasma treatment, some dislocations and stacking faults are present in the HRTEM images of the Co$_9$S$_8$ nanoparticles (Fig. S3, ESI†). It is deduced that the recrystallization would occur on the Co$_9$S$_8$ nanoparticles when treated at the high temperature of 700 °C, and the use of plasma would initialize the defect generation as reported elsewhere.[39] Fig. 1d shows the SEM image of N-Co$_9$S$_8$/G. We can see that the N-Co$_9$S$_8$ nanoparticles are homogeneously anchored on the surface of graphene. Like the TEM characterizations, the defective holes are also observed on graphene. All of the microscopy images demonstrate that the NH$_3$-plasma treatment could not only etch the graphene surface but also etch the Co$_9$S$_8$ nanoparticles, and the presence of the defects would probably be helpful to improve the electrochemical performance for ORR and OER.

Raman spectroscopy is an efficient tool to investigate the defect level of carbon materials. We collected the Raman spectrum of N-Co$_9$S$_8$/G and made a comparison with the untreated Co$_9$S$_8$/G. From Fig. 2a, we can see that there are mainly two peaks in the samples, located at approximately 1350 and 1590 cm^{-1}, corresponding to D-band and G-band, respectively. The intensity ratio of D-band to G-band can reveal the defect level of carbon nanomaterials.[40] The intensity ratio of N-Co$_9$S$_8$/G (1.42) is higher than that of Co$_9$S$_8$/G (1.15), and this reveals that the defect level of Co$_9$S$_8$/G increases after NH$_3$-plasma treatment resulting from the etching and doping effect, consistent with the SEM and TEM characterizations. Raman spectra under the 632 nm laser as given in Fig. S4 (ESI†) exhibit that the intensity ratio of N-Co$_9$S$_8$/G (1.63) is higher than that of Co$_9$S$_8$/G (1.47) as

Scheme 1 Illustration of the preparation of N-Co$_9$S$_8$/G.
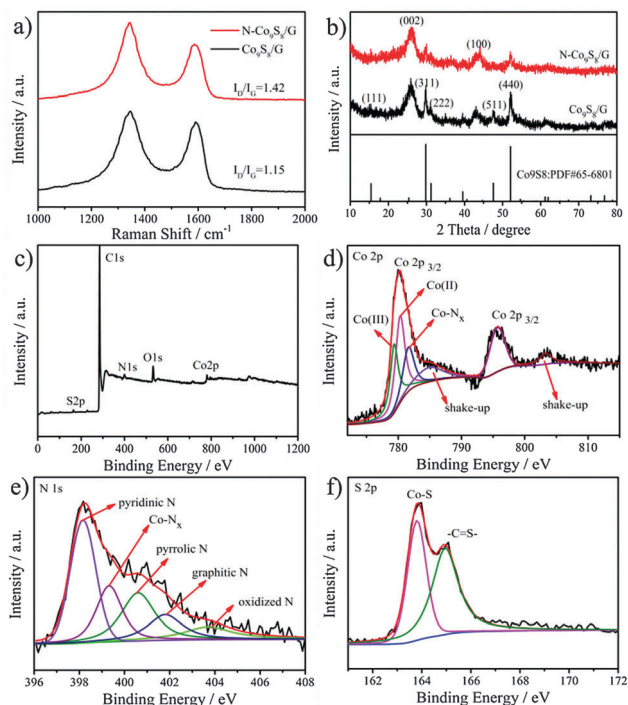
1322 | Energy Environ. Sci., 2016, 9, 1320–1326

This journal is © The Royal Society of Chemistry 2016

Fig. 2 Raman spectra of N-Co_9S_8/G and Co_9S_8/G (a); XRD patterns of Co_9S_8/G and N-Co_9S_8/G (b); the XPS survey of N-Co_9S_8/G (c), and high resolution of Co 2p XPS peak (d), N 1s XPS peak (e) and S 2p XPS peak (f).

well, indicating that the etching and doping might increase the defect level of Co_9S_8/G. To confirm the etching effect of the plasma process on graphene, Ar plasma was also employed to modify Co_9S_8/G nanoparticles (denoted as Ar–Co_9S_8/G). As shown in Fig. S5 (ESI†), it could be found that the intensity ratio of D-band to G-band of Ar–Co_9S_8/G (1.54) is also larger than that of Co_9S_8/G, indicating that more defects were generated by the plasma treatment. From the above results, we could conclude that no matter under NH_3 or Ar plasma, the etching effect could occur on the graphene surface to produce more defects as the catalytic active sites.

The crystalline structure of N-Co_9S_8/G was further characterized with XRD. As shown in Fig. 2b, the main diffraction peaks at 2θ of 15.4°, 29.8°, 31.2°, 47.5° and 52.0° in both N-Co_9S_8/G and Co_9S_8/G can be assigned to the lattice planes of (111), (311), (222), (511), and (440) of Co_9S_8 (PDF#65-6801), respectively. By comparing the XRD patterns of N-Co_9S_8/G and Co_9S_8/G, we can see that the degree of crystallization of the N-Co_9S_8/G decreases relative to that of Co_9S_8/G as evidenced by the weakened intensity of the diffraction peaks (Fig. 2b). This indicates that the NH_3-plasma treatment could partially etch the Co_9S_8 nanoparticles.

By the use of NH_3-plasma, N atoms could be successfully doped into the Co_9S_8 crystal and graphene carbon lattice which was evidenced by the XPS analysis. Fig. 2c shows the XPS survey of the N-Co_9S_8/G. It can be seen that the C, N, O, Co, and S signals are present at 284.52, 398.33, 532.3, 780.15, and 163.96 eV, respectively. The presence of O element is probably due to the absorbed oxygen-species or the residual oxygen-containing groups in the graphene. In the high resolution spectrum of the

Co 2p region (Fig. 2d), the Co $2p_{3/2}$ and Co $2p_{1/2}$ peaks are deconvoluted into four components. The peaks at 779.36, 781.61, and 784.88 eV are corresponding to the Co(III), Co(II), and the shake-up, respectively, which agree with the previous reports.[41,42] More importantly, the peak at 780.3 eV can be attributed to the cobalt with N in the Co–N_x structure.[43,44] The presence of Co–N_x clearly confirms that N atoms were doped into the Co_9S_8 lattice through the NH_3-plasma treatment. The etched and doped Co_9S_8 in this study was expected to enhance the electrocatalytic activity for ORR and OER.[35] In addition, not only in the Co_9S_8 crystal but also in the graphene carbon lattice, we could find the doped N atoms. In the N 1s XPS peaks (Fig. 2e), the Co–N_x structure could also be observed at the binding energy of 399.4 eV.[43] In addition, the N 1s peak could be further deconvoluted into another four peaks, which are pyridinic N (398.15 eV), pyrrolic N (400.59 eV), graphitic N (401.79 eV), as well as the oxidized N (403.69 eV).[45] Fig. S6 (ESI†) shows that the C–N bond (285.8 eV) exists in the high resolution XPS spectrum of the C 1s peaks after NH_3-plasma treatment. All these evidences demonstrate that N atoms have been doped into the graphene lattice successfully. The doped N atoms in graphene with the types of pyridinic N and graphitic N have a positive effect on the ORR performance of N-Co_9S_8/G and the total content of the two types is 59.1%. In the S 2p spectrum (Fig. 2f), the peak at 163.8 eV agrees with the Co–S bond. Surprisingly, a peak at the binding energy of about 165.0 eV, which is attributed to the –C≡S– bond, could be found.[46] This bond may be due to the excess S^{2-} in the Na_2S which was doped into the graphene during the hydrothermal synthesis of Co_9S_8/G. In a word, the XPS results indicate that the doped N atoms are not only in the graphene carbon lattice but also in the Co_9S_8 crystal after NH_3-plasma treatment.

Fig. S7 (ESI†) shows the thermogravimetric analysis (TGA) curves of N-Co_9S_8/G and Co_9S_8/G in the air atmosphere. We can see that the main weight loss temperatures for both the samples are in the range of 450–570 °C. More importantly, compared to the Co_9S_8/G, the final amount of residue at 800 °C decreased by 6.2 wt% for N-Co_9S_8/G, confirming the loss of Co_9S_8 after the NH_3-plasma etching. Obviously, the plasma treatment could partially etch and even remove the Co_9S_8 nanoparticles from the graphene support. This result is consistent with the TEM and XRD characterizations.

To evaluate the ORR activity, cyclic voltammograms (CVs) were carried out in N_2 and O_2-saturated 0.1 M KOH solution on different electrodes (NG, Co_9S_8, Co_9S_8/G, N-Co_9S_8, and N-Co_9S_8/G) using a three electrode system at a scan rate of 50 mV s^{-1}, as shown in Fig. 3a. Obviously, all the five electrocatalysts show a substantial oxygen reduction process in O_2-saturated electrolyte but not in N_2-purged solution, while the reduction peak potentials for the hybrid electrodes (N-Co_9S_8/G and Co_9S_8/G) are more positive than the individual NG, Co_9S_8, and N-Co_9S_8 due to the synergetic effect between Co_9S_8 and graphene. Compared to the unmodified Co_9S_8/G (0.69 V), the peak potential of ORR on N-Co_9S_8/G positively shifts to a higher potential (0.704 V) indicating the better ORR performance induced by the NH_3-plasma etching and doping. Comparing the onset potential of the two electrodes, a positive
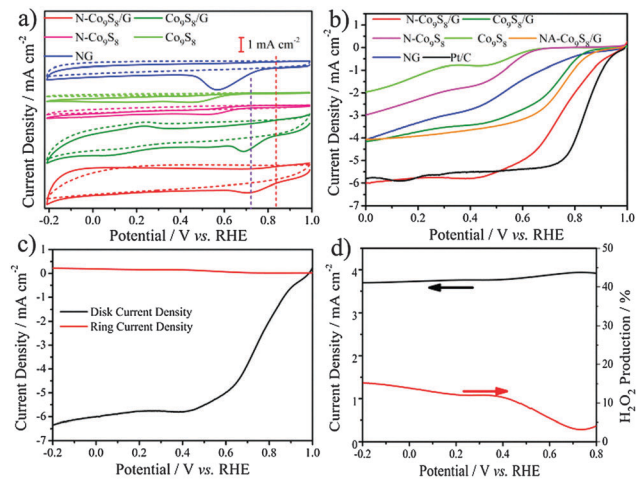
Fig. 3 (a) Cyclic voltammograms of ORR at a scan rate of 50 mV s^{-1} in N$_2$ and O$_2$-saturated 0.1 M KOH aqueous solution; (b) linear sweep voltammetry curves for ORR at a rotational speed of 1600 rpm at a scan rate of 10 mV s^{-1} in O$_2$-saturated 0.1 M KOH aqueous solution on NG, Co$_9$S$_8$, Co$_9$S$_8$/G, N-Co$_9$S$_8$, NA-Co$_9$S$_8$/G and N-Co$_9$S$_8$/G electrodes; (c) the ring current and disk current on N-Co$_9$S$_8$/G electrode at rotational speed of 1600 rpm at a scan rate of 10 mV s^{-1} in O$_2$-saturated 0.1 M KOH aqueous solution; (d) the electron transfer number and H$_2$O$_2$ production yields of ORR on N-Co$_9$S$_8$/G.

shift could be seen as well. In order to demonstrate the enhancement of ORR performance by NH$_3$-plasma treatment, we carried out CVs on the unsupported Co$_9$S$_8$ and N-Co$_9$S$_8$. Although the two electrodes without graphene support show poor ORR activity, the improvement by the plasma treatment could be seen in terms of both the peak and the onset potential. This further confirms that, NH$_3$-plasma is an efficient tool to enhance the electrocatalytic activity by N doping and surface etching. The doping with N atoms could modify the charge density on the hybrid electrocatalyst and weaken the adsorption of reaction intermediates (O and OOH) to improve the ORR performance.[38] On the other hand, plasma treatment could etch the Co$_9$S$_8$ crystal and graphene surface to gain more defects. As demonstrated by our previous reports,[31,32] the more active sites result in the better electrocatalytic performance.

Fig. 3b shows the linear sweep voltammetry (LSV) curves on a rotating disk electrode (RDE) recorded at a scan rate of 10 mV s^{-1} in O$_2$-saturated 0.1 M KOH with the rotation rate of 1600 rpm. The N-Co$_9$S$_8$/G shows the best ORR performance among the as-prepared materials with a typical one-step, four-electron pathway. The onset potential of N-Co$_9$S$_8$/G (0.941 V) is more positive than that of Co$_9$S$_8$/G (0.84 V), indicating the positive effect towards ORR through doping and etching by NH$_3$-plasma treatment. This improvement on ORR activity could also be confirmed by the comparison between Co$_9$S$_8$ and N-Co$_9$S$_8$. After treatment by NH$_3$-plasma, N-Co$_9$S$_8$ shows improved ORR performance. Co$_9$S$_8$ deposited on NG was also employed to compare with N-Co$_9$S$_8$/G, to further investigate the effect of N-doping on the Co$_9$S$_8$ nanoparticles (see Fig. S8, ESI†). As expected, without the N-doping and etching effect on Co$_9$S$_8$ nanoparticles, the ORR performance of Co$_9$S$_8$/NG is poorer than that of N-Co$_9$S$_8$/G. In addition, the Co$_9$S$_8$/NG catalyst also shows better performance than Co$_9$S$_8$/G in terms of half-wave potential for ORR. Furthermore, to investigate the

influence of defects caused by the plasma, we annealed the Co$_9$S$_8$/G in NH$_3$ atmosphere without plasma treatment (denoted as NA-Co$_9$S$_8$/G, Fig. 3b). The better performance of NA-Co$_9$S$_8$/G than that of Co$_9$S$_8$/G indicates the enhanced effect of N doping, while poorer performance in comparison with the N-Co$_9$S$_8$/G further confirms that the defects are helpful to improve the ORR performance. Remarkably, the LSV profile of N-Co$_9$S$_8$/G is similar to that of commercial Pt/C with similar onset potential and limiting diffusion current, suggesting a possible replacement for the Pt/C catalyst. However, the half-wave potential of ORR on N-Co$_9$S$_8$/G still can't catch up with the Pt/C catalyst which is a crucial problem needed to be solved in future study. On the other hand, to further investigate the synergetic effect and etching effect, a mixed gas of NH$_3$ (50%) and Ar (50%) as well as pure Ar plasma were employed to treat the Co$_9$S$_8$/G, which were denoted as (Ar + NH$_3$)–Co$_9$S$_8$/G and Ar–Co$_9$S$_8$/G, respectively. In Fig. S8 (ESI†), we can see that Ar–Co$_9$S$_8$/G exhibits a more positive onset potential (0.881 V) and a higher current density than the pristine Co$_9$S$_8$/G for ORR, contributed to by the simple etching effect on the hybrid electrocatalyst by Ar plasma. However, the performance of Ar–Co$_9$S$_8$/G is still poorer than that of NH$_3$-plasma treated Co$_9$S$_8$/G samples, indicating the role of N doping. Besides, (Ar + NH$_3$)–Co$_9$S$_8$/G exhibits slightly poorer performance than the N-Co$_9$S$_8$/G due to the low NH$_3$ concentration. These results further confirm the important role of N-doping in both the Co$_9$S$_8$ nanoparticles and the graphene lattice. Besides, we could also see that the ORR activity of the Co$_9$S$_8$/G electrode is much better than the pristine graphene (G), contributed to by the synergetic effect.[25] Electrochemical impedance spectroscopy (EIS) was conducted to analyze the change of the charge transfer properties of the electrocatalysts induced by the NH$_3$-plasma treatment. In Fig. S9 (ESI†), it can be seen that both N-Co$_9$S$_8$ and N-Co$_9$S$_8$/G electrodes show lower charge-transfer resistances (R_{ct}) than those of the non-treated Co$_9$S$_8$ and Co$_9$S$_8$/G. This clearly indicates that doping with N atoms in either the Co$_9$S$_8$ nanoparticles or the hybrid material could improve the electrical conductivity of the electrocatalyst.

To estimate the ORR performance of an electrocatalyst, the electron transfer number (n) and H$_2$O$_2$ production yield are very important indicators. Thus, an RRDE test of N-Co$_9$S$_8$/G was conducted (Fig. 3c) and the results were calculated according to the formulas as follows:[17,47]

$$n = \frac{4I_D}{I_D + (I_R/N)}$$

$$H_2O_2\% = 100 \times \frac{4 - n}{2}$$

where n is the electron transfer number, H$_2$O$_2$% is the production yield during the ORR process, I_D is the absolute value of the Faradaic current at the disk, I_R is the absolute value of the ring current, and N is the collection efficiency (0.38 in this study). The final results are shown in Fig. 3d. We can see that, in the potential range from −0.2 to 0.8 V, the n value of N-Co$_9$S$_8$/G remains between 3.7 and 3.9. This clearly reveals that the ORR on N-Co$_9$S$_8$/G follows an efficient one-step, four-electron pathway over the entire potential range with a low H$_2$O$_2$ production yield.

1324 | Energy Environ. Sci., 2016, 9, 1320–1326

This journal is © The Royal Society of Chemistry 2016

The methanol tolerance and electrochemical stability are very important for ORR electrocatalysts. We performed chronoamperometric responses for both N-Co$_9$S$_8$/G and Pt/C electrodes with addition of 1.0 M methanol (Fig. S10a, ESI†). Once methanol was injected into the electrolyte, the N-Co$_9$S$_8$/G shows a negligible decrease. While, in contrast, the current of the commercial Pt/C electrocatalyst decreases obviously, indicating an excellent methanol tolerance of the N-Co$_9$S$_8$/G electrocatalysts. The electrochemical stability was also evaluated by chronoamperometry in O$_2$-saturated 0.1 M KOH solution at 0.79 V (Fig. S10b, ESI†). After 20 000 s, the N-Co$_9$S$_8$/G electrode still retains good stability with a current loss of only 5.7%. However, the corresponding current loss on the commercial Pt/C electrode reaches up to 23.1%, indicating its poor durability in the long-term operation. Thus, the results confirm that the as-prepared N-Co$_9$S$_8$/G exhibits better methanol tolerance and electrochemical stability than the Pt/C electrocatalyst.

Similar to the ORR measurement, the OER performance investigation of the NH$_3$-plasma treated electrocatalysts was also carried out by dropping the catalyst slurry onto a rotating disk electrode (RDE) with a mass loading of 0.2 mg cm^{-2} in the O$_2$-saturated 0.1 M KOH and the rotation rate was 1600 rpm. The conventional RuO$_2$/C electrocatalyst was also tested for comparison. The Ohmic potential drop losses of all the electrodes have been corrected by *iR* compensation. As seen in Fig. 4a, the typical polarization curve of the N-Co$_9$S$_8$/G reveals a low onset potential of ∼1.51 V and a greater catalytic current than the unmodified electrodes. The NG exhibits a sluggish OER activity while RuO$_2$/C shows the lowest onset potential. Notably, after NH$_3$-plasma treatment, OER performance on both N-Co$_9$S$_8$/G and N-Co$_9$S$_8$ are enhanced like that for the ORR. This indicates that the doping and etching process through plasma treatment for the enhancement of OER activity is also effective, as the

doping process improves the electrical conductivity and the etching process increases the number of catalytic active sites. It is very meaningful to compare the overpotential requirements for achieving the current density of 10 mA cm^2.[48] We measured the overpotential of all the electrocatalysts and the results are illustrated in Fig. 4b. The N-Co$_9$S$_8$/G, NA-Co$_9$S$_8$/G and Co$_9$S$_8$/G electrodes show low overpotentials of only 0.409, 0.441 and 0.433 V, respectively. If the Co$_9$S$_8$ electrocatalyst was not anchored on graphene, the OER activity is poor due to the absence of a conductive substrate. But the improvement is also observed for N-Co$_9$S$_8$ relative to Co$_9$S$_8$ (the overpotential decreases from 0.602 to 0.548 V) after the plasma treatment.

To further investigate the OER kinetics of the as-prepared catalysts discussed above, Tafel plots were fitted according to the polarization curves (Fig. 4c). N-Co$_9$S$_8$/G shows the smallest Tafel slope of 82.7 mV dec^{-1} among the electrocatalysts and this is the intrinsic reason why N-Co$_9$S$_8$/G exhibits an efficient OER activity. Although the RuO$_2$/C shows the lowest overpotential (Fig. 4b), the Tafel slope (157.5 mV dec^{-1}) of RuO$_2$/C is much higher than that of N-Co$_9$S$_8$/G, confirming the advantage of the as-designed N-Co$_9$S$_8$/G electrocatalyst. The catalyst stability is also an important property for an OER electrocatalyst. We performed the stability test of N-Co$_9$S$_8$/G by continuous cycling CVs from 1.4 V to 1.7 V *vs.* RHE for 2000 cycles at a constant scan rate of 100 mV s^{-1}. It can be seen from Fig. 4d that, after 2000 cycles, the polarization curve for the N-Co$_9$S$_8$/G electrocatalyst shows a similar onset potential to the initial one with a slightly positive shift to a higher potential. Generally speaking, the result reveals the good stability of N-Co$_9$S$_8$/G in alkaline conditions.

Conclusions

In summary, we, for the first time, realized the simultaneous etching and N-doping of the hybrid Co$_9$S$_8$/graphene electrocatalysts, which show advanced electrocatalytic performance for both ORR and OER. The NH$_3$-plasma process used in this study has been demonstrated to be an efficient strategy for doping heteroatoms and producing more edge active sites on the surface of the hybrid electrocatalyst, and thus the as-prepared N-Co$_9$S$_8$/G exhibited highly efficient activity towards ORR and OER. The NH$_3$-plasma treatment on Co$_9$S$_8$/G could not only lead to nitrogen doping into both Co$_9$S$_8$ and graphene, but also partial etching of the surface of both Co$_9$S$_8$ and graphene. The heteroatom doping could efficiently tune the electronic properties of Co$_9$S$_8$ and graphene, and the surface etching could expose more active sites for electrocatalysis, which can contribute significantly to the enhanced electrocatalytic performance for ORR and OER. The electrochemical measurements revealed that, after NH$_3$-plasma treatment, both the ORR and OER performance of N-Co$_9$S$_8$/G could be obviously enhanced. Additionally, the N-Co$_9$S$_8$/G also showed excellent fuel selectivity and long-term durability. The electrochemical results revealed that the etched and N-doped Co$_9$S$_8$/G shows excellent ORR activity, which is close to the commercial Pt/C catalyst, and great OER activity. The strategy developed here
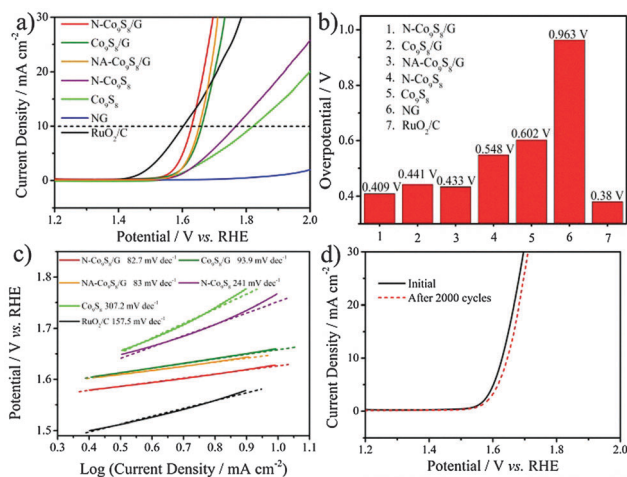

Fig. 4 (a) Linear sweep voltammetry curves for OER at 1600 rpm at a scan rate of 10 mV s^{-1} in O$_2$-saturated 0.1 M KOH aqueous solution on 20% Pt/C, NG, Co$_9$S$_8$, Co$_9$S$_8$/G, N-Co$_9$S$_8$, and N-Co$_9$S$_8$/G electrodes; the corresponding overpotentials (b) at current density of 10 mA cm^{-2} and Tafel plots (c) of RuO$_2$/C, NA-Co$_9$S$_8$/G, Co$_9$S$_8$, Co$_9$S$_8$/G, N-Co$_9$S$_8$, and N-Co$_9$S$_8$/G electrodes; (d) polarization curves for the N-Co$_9$S$_8$/G hybrid electrocatalyst before and after 2000 cycles.

This journal is © The Royal Society of Chemistry 2016

Energy Environ. Sci., 2016, **9**, 1320–1326 | **1325**

provides a novel and efficient approach to prepare hybrid bi-functional electrocatalysts for ORR and OER.

Acknowledgements

Notes and references

1 Y. Jiao, Y. Zheng, M. Jaroniec and S. Z. Qiao, *Chem. Soc. Rev.*, 2015, **44**, 2060–2086.

2 Y. Hou, Z. Wen, S. Cui, S. Ci, S. Mao and J. Chen, *Adv. Funct. Mater.*, 2015, **25**, 872–882.

3 Z.-L. Wang, D. Xu, J.-J. Xu and X.-B. Zhang, *Chem. Soc. Rev.*, 2014, **43**, 7746–7786.

4 Z.-L. Wang, D. Xu, H.-X. Zhong, J. Wang, F.-L. Meng and X.-B. Zhang, *Sci. Adv.*, 2015, **1**, e1400035.

5 G. Zhang, C. Li, J. Liu, L. Zhou, R. Liu, X. Han, H. Huang, H. Hu, Y. Liu and Z. Kang, *J. Mater. Chem. A*, 2014, **2**, 8184–8189.

6 G. L. Tian, M. Q. Zhao, D. Yu, X. Y. Kong, J. Q. Huang, Q. Zhang and F. Wei, *Small*, 2014, **10**, 2251–2259.

7 H. x. Zhong, J. Wang, Y. w. Zhang, W. l. Xu, W. Xing, D. Xu, Y. f. Zhang and X. b. Zhang, *Angew. Chem., Int. Ed.*, 2014, **53**, 14235–14239.

8 W. T. Hong, M. Risch, K. A. Stoerzinger, A. Grimaud, J. Suntivich and Y. Shao-Horn, *Energy Environ. Sci.*, 2015, **8**, 1404–1427.

9 C. Xu, M. Lu, Y. Zhan and J. Y. Lee, *RSC Adv.*, 2014, **4**, 25089–25092.

10 E. Antolini, *ACS Catal.*, 2014, **4**, 1426–1440.

11 J. Wang, K. Li, H. x. Zhong, D. Xu, Z. l. Wang, Z. Jiang, Z. j. Wu and X. b. Zhang, *Angew. Chem., Int. Ed.*, 2015, **54**, 10530–10534.

12 J. Liang, Y. Jiao, M. Jaroniec and S. Z. Qiao, *Angew. Chem., Int. Ed.*, 2012, **51**, 11496–11500.

13 S. Y. Huang, P. Ganesan, H. Y. Jung and B. N. Popov, *J. Power Sources*, 2012, **198**, 23–29.

14 S. Rivas, L. G. Arriaga, L. Morales and A. M. Fernandez, *Int. J. Electrochem. Sci.*, 2012, **7**, 3601–3609.

15 F. D. Kong, S. Zhang, G. P. Yin, N. Zhang, Z. B. Wang and C. Y. Du, *Electrochem. Commun.*, 2012, **14**, 63–66.

16 K. Gong, F. Du, Z. Xia, M. Durstock and L. Dai, *Science*, 2009, **323**, 760–764.

17 S. Wang, E. Iyyamperumal, A. Roy, Y. Xue, D. Yu and L. Dai, *Angew. Chem., Int. Ed.*, 2011, **50**, 11756–11760.

18 S. Wang, L. Zhang, Z. Xia, A. Roy, D. W. Chang, J. B. Baek and L. Dai, *Angew. Chem., Int. Ed.*, 2012, **51**, 4209–4212.

19 X. Wang, J. Wang, D. Wang, S. Dou, Z. Ma, J. Wu, L. Tao, A. Shen, C. Ouyang and Q. Liu, *Chem. Commun.*, 2014, **50**, 4839–4842.

20 R. Li, Z. Wei and X. Gou, *ACS Catal.*, 2015, **5**, 4133–4142.

21 S. Chen, J. Duan, J. Ran and S. Z. Qiao, *Adv. Sci.*, 2015, **2**, DOI: 10.1002/advs.201400015.

22 L. Wang, F. Yin and C. Yao, *Int. J. Hydrogen Energy*, 2014, **39**, 15913–15919.

23 G. S. Hutchings, Y. Zhang, J. Li, B. T. Yonemoto, X. Zhou, K. Zhu and F. Jiao, *J. Am. Chem. Soc.*, 2015, **137**, 4223–4229.

24 Z. Han, Z. Junfeng, Y. Ruoping, D. Mingliang, W. Qingfa, G. Guohua, W. Jiong, W. Guangming, Z. Ming and L. Bo, *Adv. Mater.*, 2015, **27**, 4752–4759.

25 Y. Liang, Y. Li, H. Wang, J. Zhou, J. Wang, T. Regier and H. Dai, *Nat. Mater.*, 2011, **10**, 780–786.

26 B. Hu, Z. Jing, J. Fan, G. Yao and F. Jin, *Catal. Today*, 2016, **263**, 128–135.

27 G. Wu, H. T. Chung, M. Nelson, K. Artyushkova, K. L. More, C. M. Johnston and P. Zelenay, *ECS Trans.*, 2011, **41**, 1709–1717.

28 G. Wu, N. H. Mack, W. Gao, S. Ma, R. Zhong, J. Han, J. K. Baldwin and P. Zelenay, *ACS Nano*, 2012, **6**, 9764–9776.

29 Q. Liu, J. Jin and J. Zhang, *ACS Appl. Mater. Interfaces*, 2013, **5**, 5002–5008.

30 U. L. Dong, B. J. Kim and Z. Chen, *J. Mater. Chem. A*, 2013, **1**, 4754–4762.

31 L. Tao, X. Duan, C. Wang, X. Duan and S. Wang, *Chem. Commun.*, 2015, **51**, 7470–7473.

32 A. Shen, Y. Zou, Q. Wang, R. A. Dryfe, X. Huang, S. Dou, L. Dai and S. Wang, *Angew. Chem.*, 2014, **53**, 10804–10808.

33 L. Zhang, J. Niu, L. Dai and Z. Xia, *Langmuir*, 2012, **28**, 7542–7550.

34 H. Yu, Y. Li, X. Li, L. Fan and S. Yang, *Chemistry*, 2014, **20**, 3457–3462.

35 R. Asahi, T. Morikawa, T. Ohwaki, K. Aoki and Y. Taga, *Science*, 2001, **293**, 269–271.

36 X. Yang, A. Wolcott, G. Wang, A. Sobo, R. Fitzmorris, F. Qian, J. Zhang and Y. Li, *Nano Lett.*, 2009, **9**, 2331–2336.

37 D. Shuo, H. Xiaobing, M. Zhaoling, W. Jianghong and W. Shuangyin, *Nanotechnology*, 2015, **26**, 045402.

38 X. Zhong, L. Liu, Y. Jiang, X. Wang, L. Wang, G. Zhuang, X. Li, D. Mei, J. G. Wang and D. S. Su, *ChemCatChem*, 2015, **7**, 1826–1832.

39 K. Morita, B. N. Kim, H. Yoshida, K. Hiraga and Y. Sakka, *Acta Mater.*, 2015, **84**, 9–19.

40 S. Dou, A. Shen, L. Tao and S. Wang, *Chem. Commun.*, 2014, **50**, 10672–10675.

41 J. Pu, Z. Wang, K. Wu, N. Yu and E. Sheng, *Phys. Chem. Chem. Phys.*, 2013, **16**, 785–791.

42 S. Yunhe, Z. Yihua, J. Hongliang, S. Jianhua, Y. Xiaoling, Z. Wenjian, C. Jianding and L. Chunzhong, *Nanoscale*, 2014, **6**, 15080–15089.

43 K. Niu, B. Yang, J. Cui, J. Jin, X. Fu, Q. Zhao and J. Zhang, *J. Power Sources*, 2013, **243**, 65–71.

44 Z. Liu, L. Ji, X. Dong, Z. Li, L. Fu and Q. Wang, *RSC Adv.*, 2014, **5**, 6259–6264.

45 C. Zhang, R. Hao, H. Liao and Y. Hou, *Nano Energy*, 2013, **2**, 88–97.

46 J. Y. Lin, J. H. Liao and S. W. Chou, *Electrochim. Acta*, 2011, **56**, 8818–8826.

47 J. Zhu, C. He, Y. Li, S. Kang and P. K. Shen, *J. Mater. Chem. A*, 2013, **1**, 14700.

48 L. Wu, Q. Li, C. H. Wu, H. Zhu, A. Mendoza-Garcia, B. Shen, J. Guo and S. Sun, *J. Am. Chem. Soc.*, 2015, **137**, 7071–7074.

1326 | *Energy Environ. Sci.*, 2016, **9**, 1320–1326

This journal is © The Royal Society of Chemistry 2016